Journal of Structural Geology, Vol. 11, No. 7, pp. 859 to 871, 1989
Printed in Great Britain

0191-8141/89 $03.00 + 0.00

Deformational behavior of shale interlayers in evaporite detachment horizons, Jura overthrust, Switzerland

PETER JORDAN

Geological Institute, The University, CH-4056 Basel, Switzerland

and

ROLF NÜESCH*

Geological Institute, ETH, CH-8092 Zürich, Switzerland

(*Received* 1 *November* 1988; *accepted in revised form* 16 *May* 1989)

Abstract—Shale deformation was studied in a series of naturally strained evaporites and shales deformed at low temperatures ($\leq 70°$), high strain rates ($\geq 5 \times 10^{-14}\ s^{-1}$) and low pressures (overburden <2 km), as well as in rock samples and sintered specimens experimentally deformed in coaxial and simple shear configurations at temperatures of 20–350°C, strain rates of 10^{-4}–$10^{-6}\ s^{-1}$ and confining pressures of 0.1–400 MPa.

Within naturally strained shale–sulfate multilayers, three deformation regimes can be recognized; that are separated by the inversion of relative competence of shale and anhydrite and the onset of gypsification, respectively. In deeper domains strain is focused on slickensides, which are often coated with sulfate that acts as a lubricant. In shallower domains, and especially in domains with significant access to syntectonic water, strain becomes pervasive and very low-strength 'ductile' 'shale–gypsum-tectonites' form.

Experiments reveal that confining pressure and water content have a significant influence on style of deformation (pervasive or focused on discrete surfaces), whereas temperature and strain rate have virtually no influence on either strength or deformation style, except at temperatures >200°C that cause dehydration and embrittlement.

INTRODUCTION

BOTH shales and evaporites are important decoupling materials in deformational structures of all scales (e.g. Laubscher 1961, Cooper 1970, Harris & Milici 1977, Ramsay 1981, Helman & Schreiber 1983, van Berkel *et al.* 1986, Marcoux *et al.* 1987, Harland 1988). The main reason for decoupling in evaporites is the very low strength, for ductile flow of halite (e.g. Heard 1972, Carter & Hansen 1983), anhydrite (Müller *et al.* 1981), gypsum (Baumann 1984) and other evaporite components (e.g. Urai 1985). In shales, however, friction-controlled slip along discrete surfaces and cataclastic flow is considered to be the dominant deformation mechanism (Handin *et al.* 1963, Wang *et al.* 1980, Logan *et al.* 1981, Maltman 1984, 1987, Nüesch 1989). Furthermore, the frictional strength of shales is distinctly lower than the corresponding strengths of all other common rock types (Byerlee 1978).

In order to investigate the direct competitiveness of shales and evaporites (anhydrite, gypsum) as decoupling materials under various ambient conditions we have, in recent years, examined several configurations where these materials are interlayered within evaporite sequences (Jordan 1987, 1988, Jordan & Nüesch 1989, Nüesch & Baumann 1989). In this paper we concentrate on the deformational behavior of shale interlayers in sulfates and address three subjects: (a) the peculiarities of shale deformation in evaporites; (b) the role of friction in shale deformation and the factors decisive in determining whether deformation is friction-controlled or frictionless; and (c) the deformational behavior of evaporites as a polyphase system, particularly with respect to the influence of specific shale deformation mechanisms. This paper is based on a recent experimental study on the mechanical properties of shales (Nüesch 1989), on experimental data for anhydrite (Müller *et al.* 1981) and gypsum (Baumann 1984), and on field investigations in the most prominent decoupling horizons of the Jura.

The Jura is the front of the youngest and most external nappe of the Alpine system. During the late Miocene and Pliocene, the subduction of the European basement under the Alpine arc caused a northward décollement of the Alpine foreland sedimentary wedge (Fig. 1) (Buxtorf 1907, Laubscher 1961, 1973–'Fernschub concept', Hsü 1979). The (older) Muschelkalk evaporites acted as the main décollement (e.g. Müller *et al.* 1984, Jordan & Nüesch 1989), while a second, subordinate décollement developed in the (younger) Keuper evaporites. Ductile flow, which is restricted to these evaporite sequences, was responsible for the propagation of the Jura décollement far towards the foreland (Laubscher 1961, 1976, Müller & Hsü 1980, Davis & Engelder 1985, Becker *et al.* 1987). Less important décollements are localized within the shale formations, predominantly within the Middle Jurassic Opalinus shale, which is also an important 'filler' material of anticlines ('delta structures',

* Present address: Institut für Grundbau und Bodenmechanik (Tonmineralogie), ETH, CH-8092 Zürich, Switzerland.

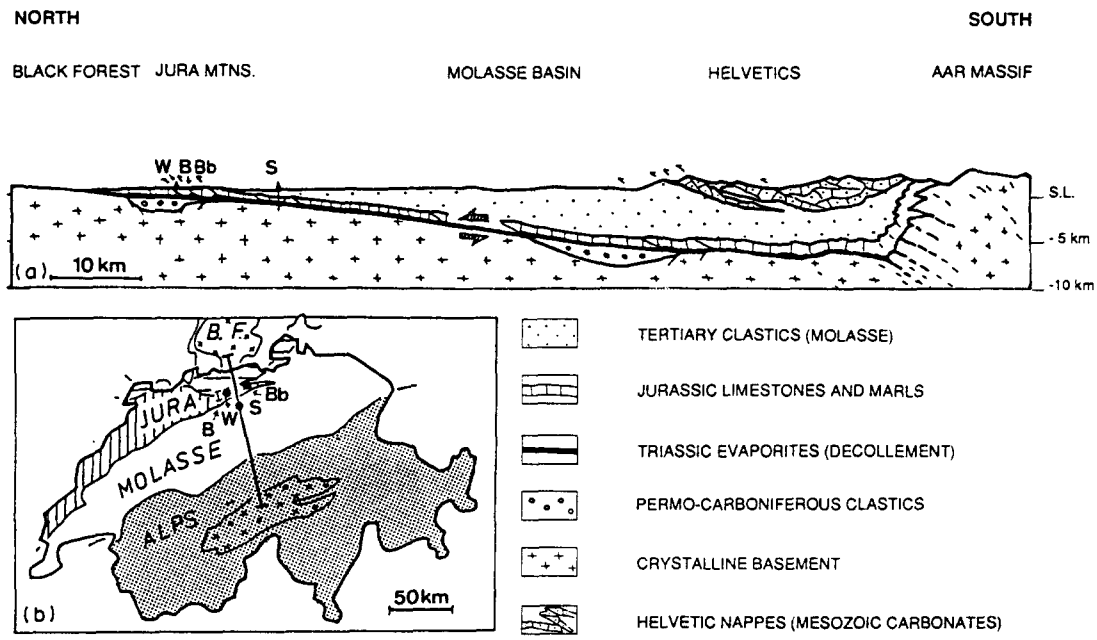

Fig. 1. (a) Cross-section from the Central Alps to the Alpine foreland (redrawn after Müller *et al.* 1984) showing the extent of the Jura Main Décollement and the sample localities: B = Belchen, Bb = Bözberg, S = Schafisheim, W = Wiesen. (b) Map to show the location of the cross-section. The heavy line is the Swiss national border.

Laubscher 1986). Outside these decoupling horizons, the dominant deformation mechanisms of Jura overthrusting were friction-controlled shear along discrete surfaces, fault brecciation, and pressure solution (Wohnlich 1967, Laubscher 1977, 1978).

For our investigations, we sampled the Muschelkalk evaporites at Schafisheim and Wiesen well, and the Keuper evaporites at the Belchen motorway tunnel. At Schafisheim, the Jura Main Décollement ('Hauptabscherhorizont') was encountered in a hinterland position with respect to the Jura proper (Jordan & Nüesch 1989). The evaporites from the recent Wiesen well originate from the Jura boundary thrust ('Randüberschiebung'), one of the most prominent detachments branching from the Main Décollement. At the Belchen motorway tunnel, the Keuper evaporites act as a roof thrust of a duplex sequence built up by the approximately 70 m thick carbonate 'Hauptmuschelkalk', which is interlayered between the two evaporite sequences (Wohnlich 1967, Laubscher 1976, 1984, Jordan 1988).

Both evaporite sequences are rich in interlayers varying from pure shales to dolomites, and ranging from several mm to several m in thickness. The clay fraction comprises illite, corrensite and chlorite (Prasad 1970, Peters *et al.* 1986, Matter *et al.* 1988). Corrensite, a swelling clay mineral which has a decisive influence on specific surface area and therefore on the rheology of shales (Nüesch 1989), makes up 10–50% of the clay fraction, and in some samples even as much as 80% (Peters *et al.* 1986, Matter *et al.* 1988). In the marly interlayers, very fine-grained dolomite and subordinate magnesite is found (Jordan & Nüesch 1989).

At Schafisheim, the ambient conditions effective during Jura overthrusting can be characterized as moderate- to high-strain rates (1.8×10^{-13}–1.3×10^{-12} s^{-1}) and low temperatures (≤80°C) and confining pressures (*ca* 45 MPa). At Belchen and Wiesen, temperatures (≤70°C) and confining pressures (*ca* ≤40 MPa) were slightly lower. At Belchen, the strain is less intense than at the two other locations, and the overall strain rate estimate is somewhat lower (*ca* 5×10^{-14}–1×10^{-12} s^{-1}).

In order to distinguish deformation patterns typical of shales proper from patterns restricted to shale interlayers in evaporites, we sampled naturally strained Opalinus shale (an arenitic and carbonaceous clay-stone that was deformed during Jura overthrusting). The samples used for laboratory work (Table 1) originate from the Bözberg well (Nüesch 1989).

FIELD OBSERVATIONS

Three deformation patterns

At least three deformation patterns can be distinguished within the shale–anhydrite multilayers of Jura evaporite shear zones. Pattern 1 is characterized by incompetent, ductilely deformed anhydrite and boudinaged shale interlayers. It is common at Schafisheim, but is also found at Wiesen and Belchen. In pattern 2, the relative competence of shales and anhydrite is reversed with respect to pattern 1. Anhydrite layers are invariably deformed ductilely, but they are boudinaged in a pinch-and-swell manner when strongly strained. Pattern 2 is quite common within the moderately deformed evaporites of the Belchen section, is also found at Wiesen, but is absent at Schafisheim. There is a broad field of transition between patterns 1 and 2. Pattern 3 is characterized by boudinaged brittle anhydrite layers within highly ductile shale–gypsum cataclasites. Pattern 3 is found at Wiesen where it is restricted to the bottom

Table 1. Mineralogical compositions and grain sizes of the lithologies used in the experiments that provided the data for the compilation of Fig. 10

	Anhydrites		Gypsum	Clay
	Wandflue type	Riburg type	Felsenau type	Bözberg type
Mineral composition (%)				
Anhydrite	95	91	*ca* 3	—
Gypsum	<1	2–3	*ca* 85	—
Dolomite	2–3	*ca* 5	—	—
Calcite	—	—	—	*ca* 10
Quartz	} *ca* 2	} *ca* 2	*ca* 8	*ca* 30
Mixed layer			—	*ca* 25 } *ca* 55
Illite			—	*ca* 10
Chlorite			*ca* 4	*ca* 10
Kaolinite			—	*ca* 10
Others	—	—	—	*ca* 5
Grain size (mm)				
Range	An: 0.05–0.1	An: 0.05–0.3	?	Cl: 0.01–0.04
Mean	An: 0.07	An: 0.12	Gy: 0.1 An: 0.01	—

and top few tens of cm of the shear zone, i.e. close to important aquifers, and at Belchen section where it is commonly associated with late thrusts, as well as in many outcrops of the frontal part of the Jura boundary thrust.

At Wiesen, where all three patterns are found, there is a clear indication from overprinting evidence that there was a transition in time from pattern 1 to pattern 3 associated with a continuous change in transport direction. This suggests that the three patterns resulted from successive changes in deformation regime during the upward movement of the hangingwall. From field evidence, it can be postulated that this sequence of deformation regimes is characterized by decreasing temperture and overburden (syntectonic denudation). Obviously, changes in the state of equilibrium between anhydrite and gypsum are closely related to changes in deformation pattern. In pattern 1, anhydrite is the only stable form of Ca-sulfate, in the country rock as well as in vein fillings. In pattern 2, gypsum successively replaces anhydrite as a vein filling, while in pattern 3 gypsum is the dominant type of Ca-sulfate, and anhydrite appears as unchanged relics in the country rock. As the state of equilibrium between anhydrite and gypsum is controlled not only by temperature and confining pressure but also by the presence and salinity of pore water (e.g. Berner 1971), these two latter factors have to be considered as equally important in determining the deformation regime.

Within the shales of patterns 1 and 2, strain is strongly concentrated along discrete surfaces. Generally, there are two types of shear surfaces: slickensides and sulfate veins. There is, however, a broad variety of intermediate structures. Nevertheless, sulfate-free and sulfate-coated shear surfaces are aligned in a well-defined geometry relative to the shear-zone boundary, resembling an *R*–*Y*-system (Fig. 2). Actually, "*R*" and "*Y*" have to be put in quotation marks because the "*R*"-surfaces formed originally not as *R*-surfaces, but as steeper surfaces which have been rotated into this stable position. During this rotation they suffered considerable amounts of extension resulting in sulfate coating. Correspondingly, the "*Y*"-surfaces, although originally in a *Y*-orientation, have been rotated into a position inclined relative to the shear-zone boundary. The intersections of "*R*"- and "*Y*"-surfaces in the shales result in lozenge-shaped bodies, varying in diameter from tenths of a mm up to some tens of cm. Many of these bodies are subdivided into geometrically similar sub-bodies (Fig. 3a).

In pattern 3, deformation becomes pervasive, resulting in large-scale shale cataclasites commonly rich in secondary gypsum. These 'shale–gypsum-tectonites' (Jordan 1988) behave as a nearly homogeneous isotropic medium, being the least competent lithology during Jura overthrusting.

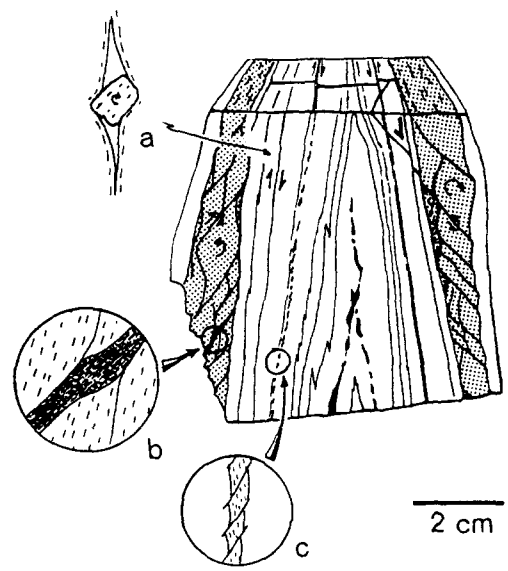

Fig. 2. Hinge of a nearly isoclinal similar fold of anhydrite (white) and shale multilayer from the Belchen section. Shales (grey, black) are dismembered into lozenge-shaped bodies by "*Y*"- and "*R*"-surfaces. Notice the symmetry of shear surfaces in both fold limbs relative to the axial plane. (a) Rotated dolomite porphyroclast in sheared anhydrite. (b) Strained anhydrite vein with mylonite-like texture. (c) Lozenge-shaped pull-aparts of a thin shale layer.

Friction-controlled processes in shale deformation

The most apparent friction-controlled processes are the formation of and the sliding along slickensides. Commonly, the slickensides in shales of Jura evaporite shear zones are characterized by highly polished, mostly planar surfaces. On irregular, undulous surfaces, polishing is most prominent on crests and depressions oriented normally to the shear direction (Fig. 5a). The mirror-like surfaces are produced by a very strong preferred orientation of the platy clay minerals or mineral aggregates parallel to the shear surface. The thickness of the slickenside domains normal to the surface, i.e. the domain of strong alignment of clay particles parallel to the slip surface, ranges from 1 to 4 μm (Fig. 3b). In these zones, commonly formed as drag zones, the packing of the clay particles is distinctly denser than in the nearby domains within the shale rhomboids. Furthermore, the average grain size of clay aggregates decreases towards the slickenside surface. In summary, the dominant deformation mechanism of shales in this deformation regime can be described as cataclasis along narrow discrete shear zones resulting in a grain-size reduction and progressive alignment of the clay minerals or mineral aggregates parallel to the shear-zone boundaries. Finally, slickensides are formed that take up all the shear movements.

At Wiesen, polished flexural-slip surfaces sporadically show polygonal structures (Figs. 3c and 5b). The polygons are outlined by small grooves or steps (20–100 μm in width or height). Accumulations of fine-grained dolomite (<10 μm) are common along these boundaries. The polygons are elongate in the direction of maximum strain, and their surfaces are nearly co-planar. This structure turns into a 'fish scale' structure when the slip surface is bent. The 'scales' are formed by inclined polygons that form distinct steps. Steps likewise associated with accumulation of fine-grained dolomite are also found outside the polygonal and scaly structures (Fig. 3d).

Striations on slickensides are common. The 20–30 μm wide striae are carved by idiomorphic feldspar and quartz grains. Within the striae, the texture of the clay minerals is roughened with respect to the original polished surfaces (Fig. 3d).

The early development of 'shale–gypsum-tectonites' was also friction-controlled as can be seen by noting the influence of secondary pore space on bulk rheology. Field evidence suggests that 'shale–gypsum-tectonites' developed from shale cataclasites. Dilatation resulted in new pore space, subsequently filled by secondary gypsum which acted as a lubricant. Generally, this process nucleated from a discrete shear zone involving progressively increasing portions of the surrounding shales. Therefore, there is a significant difference between the mechanism of slickenside development, and the mechanism responsible for the formation of 'shale–gypsum-tectonites', and this difference cannot be explained very easily. In the former case, deformation was increasingly focused on discrete shear surfaces, which in many cases were sulfate-coated. Within the nearby cataclastic zones in the periphery of the lozenge-shaped shale bodies, no sulfates precipitated. Within the 'shale–gypsum-tectonites', however, no discrete shear surfaces are found, rather the shear zones became increasingly broader with increasing strain, and there was an important precipitation of sulfates within the cataclastic zones. We suggest that four factors were responsible for this difference in behavior: the confining pressure; the presence of pore water; the chemistry of the pore water; and the mechanical behavior of the shales proper.

Brittle vs ductile deformation in shales

In the shales of evaporite shear zones, no evidence for ductile deformation in a strict sense was found. At the scale of individual clay minerals or mineral aggregates, deformation was brittle throughout the whole range of deformation regimes. On the rock scale, however, ductile deformation occurred, commonly in relation to the occurrence of secondary sulfates (sulfate-lubrication on discrete shear surfaces or gypsum-lubricated cataclasis), and this was generally related to an obvious decrease in bulk strength.

Sulfate-coating occurs in patterns 1 and 2 on both the "*Y*"- and "*R*"-surfaces, although it is more abundant on the extensive "*R*"-surfaces (Fig. 3a). Generally, sulfates started to grow as calcite step-like features, with growing directions parallel to the shear direction (Laubscher 1984). In this configuration, they acted as a perfect lubricant, provided the sulfates were less competent than the shales. In pattern 1, anhydrite was definitely less competent than shale, but even in the transition regime between regimes 1 and 2, anhydrite could have acted as a lubricant assuming pure vein anhydrite was distinctly less competent than impure country rock anhydrite. Coming into the stability field of gypsum, once again a very low-strength lubricant was available. However, in patterns 1 and 2, sulfate-free slickensides are found. This would indicate that, under certain geometri-

Fig. 3. Slickensides in shale layers of evaporite shear zones: (a) Side and top views of a group of lozenge-shaped shale bodies and sub-bodies (from the fold in Fig. 2). Notice the anhydrite-coated "*R*"-surfaces. (b) Section normal to foliation of shale layer intersected by "*R*"- and "*Y*"-surfaces. The "*R*"-shear is accompanied by a small drag zone parallel to the slickenside, showing grain-size reduction of clay aggregates. The solid seam along the shear zone and the small lozenge-shaped body in the acute angle of the shear zones both consist of clay minerals similar in chemical composition to the matrix; they are interpreted as domains of very small-sized clay aggregates smeared during sample preparation (SEM picture, Belchen). (c) Fish scale structure on flexural-slip surface (top), on which removed block moved upwards, and polygonal structure (bottom) produced by N–S flexural-slip (SEM pictures, Wiesen) cf. Fig. 5(b). (d) Striae on polished surface carved by feldspar grains (top) on which the removed block moved down; polished surface outside striae (middle left) and roughened surface inside striae (middle right) (both details of top picture); and steps associated with dolomite accumulation (bottom). (All SEM pictures, Belchen.)

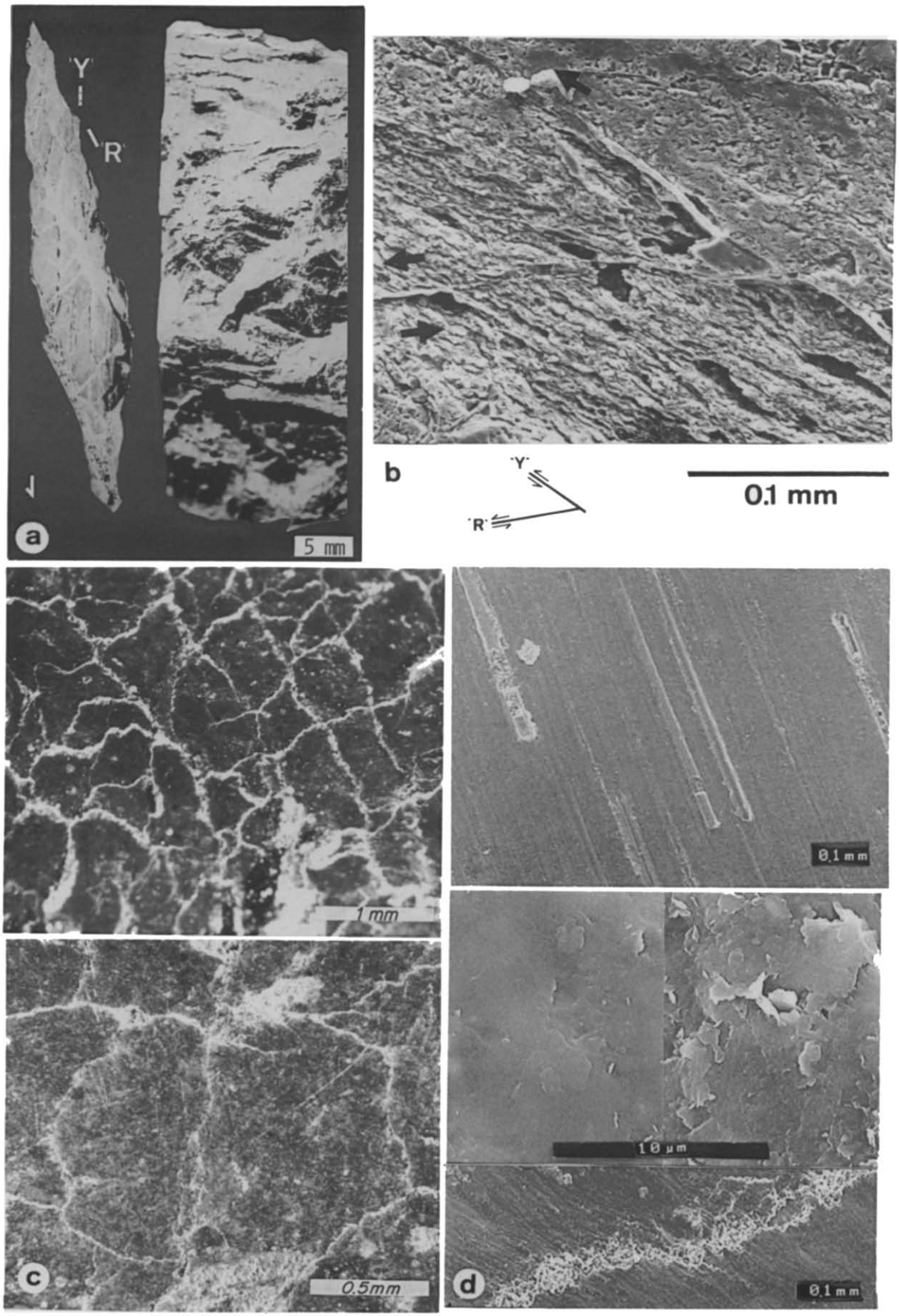
Y
R
a
5 mm
b
Y
R
0.1 mm
1 mm
0,1 mm
c
0.5mm
10 µm
d
0,1 mm

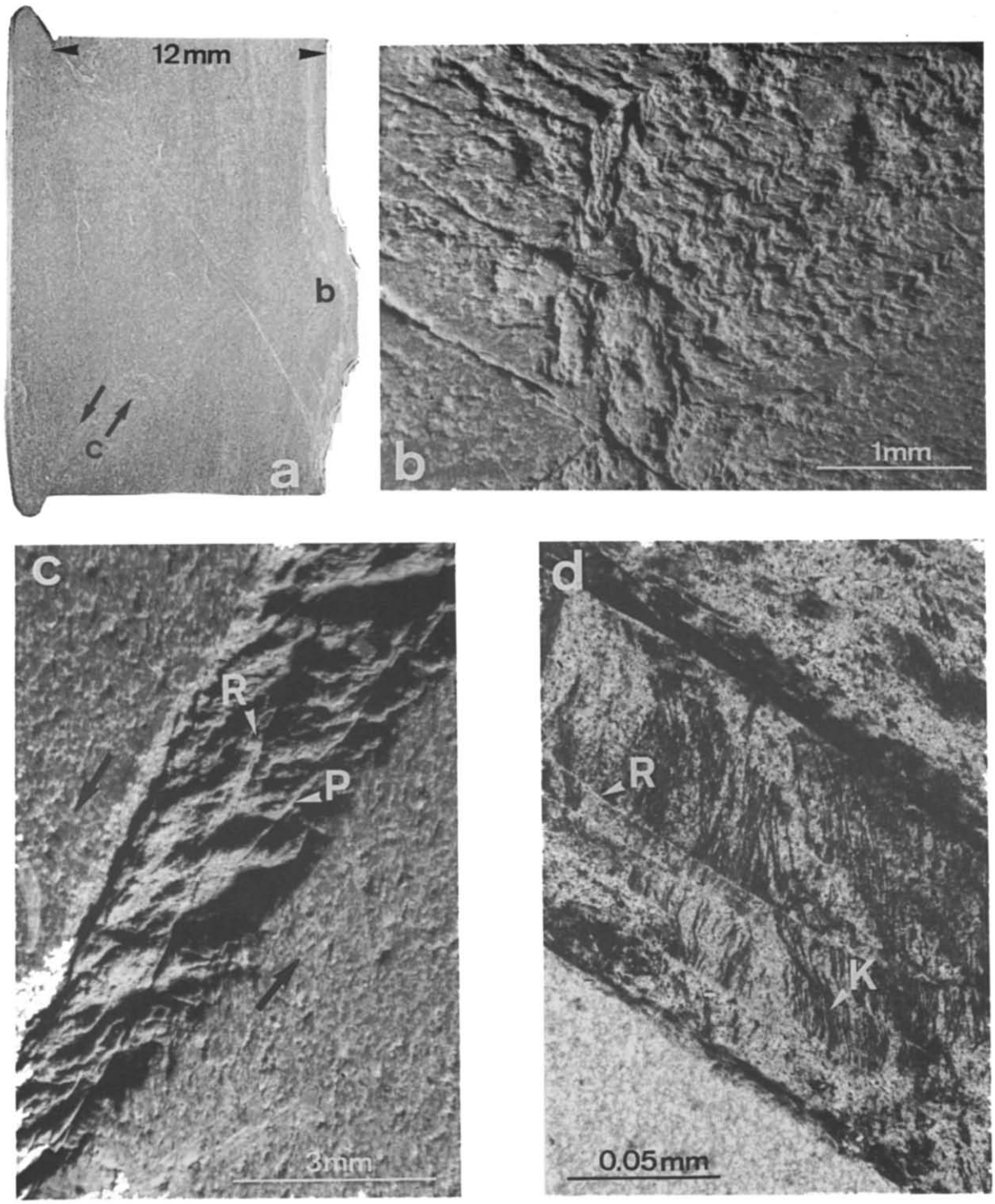

Fig. 4. Microstructures of experimentally deformed shales. (a) Intact rock sample with layering parallel to σ_1, 21% strain at 100 MPa cp, $T = 20°C$ and $\dot{\varepsilon} = 10^{-4}\,s^{-1}$. (b) Detail beneath the bulge of the deformed rock sample shows pervasive kinking. (c) Kinked shear band cut by *R*- and *P*-shears indicated. (d) Sinistrally deformed clay fraction gouge with 30 weight % water. The bulk shortening direction σ_1 is horizontal. Nicols are crossed, kingk (K) appear dark and are cut by *R*-shears (R).

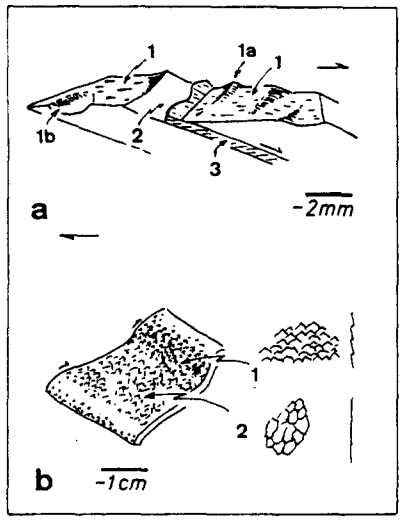

Fig. 5. Slickensides in shale layers of evaporite shear zones. (a) Slickensides on surfaces outlining lozenge-shaped bodies: undulating, polished and striated "*Y*"-surface (1) with highly polished crests (1a) and depressions (1b) oriented normal to the shear direction and "*R*"-surface (2) coated by a sulfate vein (3). (b) Polished surfaces on subordinate monocline within a flexural slip surface showing scaly structures on 'inclined' area (1) and polygonal structures on 'plane' area (2). Blow ups show details of normal view (left) and schematic cross-sections.

cal conditions, friction-controlled sliding along slickensides was competitive relative to ductile flow in sulfates. Sulfate-free slickensides are most common in "*Y*"-positions and as flexural-slip surfaces of tight folds. Both surfaces can be interpreted as transpressive.

Within the 'shale–gypsum-tectonites', friction-controlled processes were nearly totally overshadowed by ductile flow in gypsum. As outlined above, there are some significant differences in the development of slickensides and 'shale–gypsum-tectonites'. In the following, a possible genesis of the low-strength 'shale–gypsum-tectonite' is proposed. Generally, these tectonites are restricted to areas of thin overburden and to domains close to important aquifers (carbonates or thrust surfaces). This suggests their formation is favored by conditions of low confining pressure, significant water content and, possibly, excess pore pressure. Pore water in unaltered and sealed evaporites inside and outside the Jura orogenic belt has high NaCl content ("post-Stephanian salt-rich fluids", Mullis & Stalder 1987). Within the Jura, a general decrease in the NaCl-content of pore fluids during Jura overthrusting time has been documented, and this is probably the result of thrusting-induced changes in the ground water circulation to favor meteoric water access (Mullis 1987). We suggest that this low NaCl-water found its way into the evaporites when their seal was broken. This opening of the formerly closed system was possibly caused by the inversion of relative competence between anhydrite and gypsum that resulted in a consequent shifting of main shear movements from anhydrite to shales (dilatation). A low NaCl-content would depress the stability field of gypsum from a pressure equivalent to *ca* 200 m overburden (at high NaCl) to a pressure equivalent to *ca* 1.2 km overburden (at low NaCl) under the estimated ambient conditions of temperature (MacDonnald 1953, Berner 1971). As increasing pore pressure does not explain the broadening of shear zones, we suggest that accessing water changes the deformation mechanism of shales in favor of pervasive deformation. Finally, we suggest that in this deformation regime, the crystallization pressure of gypsum exceeds the swelling pressure of shales, thus explaining the deposition of gypsum within the dilatation zone of shales.

A comparison with the deformational behavior of Opalinus shale

Due to the lack of any lubricant, deformation of the Opalinus shale is predominantly brittle. Nevertheless, a large number of deformation structures comparable to those in the evaporite sequences can be found. Deformed Opalinus shale is divided by shear surfaces into lozenge-shaped bodies of various sizes. Three geometries can be distinguished: *Y–R* bounded bodies, which are common, and *R–P* and *Y–S* bounded bodies, which are rare. The *Y*- and *R*-surfaces are polished or relatively rough surfaces. Generally, they developed from kink bands, which suffered strong reduction in aggregate size. The slickensides are often depleted in carbonate which, we suggest, reduced the frictional strength. Part of the carbonate is redeposited on extensional surfaces within the shale proper. In the Opalinus shale, pervasive deformation is restricted to subsurface domains and areas of high water content. Under these conditions, shale is nearly cohesionless ('clay plasticity', see below). Therefore, the Opalinus shale differs significantly from the shales of the evaporite shear zones, where pervasive cataclasis in connection with gypsum lubrication is found at greater depths.

EXPERIMENTAL RESULTS

Generally, the mechanical behavior of the Opalinus shale (Nüesch 1989) corresponds to that of other tested shales (e.g. Handin *et al.* 1963, Chappell 1974, Summers & Byerlee 1977, Byerlee 1978, Rutter & White 1979, Wang *et al.* 1980, Logan *et al.* 1981, Rutter *et al.* 1986, Maltman 1987). In the present paper, however, we concentrate on the influence of changes in temperature, strain rate, confining pressure and water content on both strength and microstructural evolution.

Adsorbed water in Opalinus shale

The amount of adsorbed water in the shale depends on the specific surface area of the clay minerals and, therefore, on the mineral composition, as well as on the confining pressure (Madsen & Müller-Vonmoos 1985). The specific surface area of both Opalinus shale and shale interlayers in the two evaporite sequences is about 140 $m^2 g^{-1}$ (Matter *et al.* 1988). Absorption experiments (Fig. 6) yielded 1.8 weight % adsorbed water for the first bound-water layer and 4% for two, *ca* 6% for three and

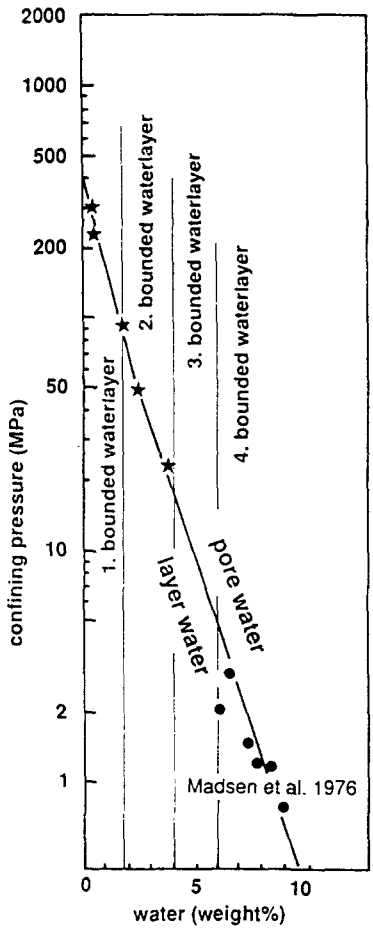

Fig. 6. Number of water interlayers as a function of confining pressure (area of clay mineral surface is 140 $m^2\ g^{-1}$). Dots indicate measurements by Madsen *et al.* (1976).

even up to 10% for four adsorbed water interlayers. Thus, 1.8% corresponds to the average water content of specimens used for experimental work (see below), while 10% is about the normal water content of natural Opalinus shale close to the surface. Starting with saturated shales, water in the fourth bound-water layer begins to be forced out as free pore water when the confining pressure exceeds 5 MPa. At 25 MPa (corresponding to *ca* 1 km depth), only two water interlayers are adsorbed, while 400 MPa is needed to remove all adsorbed water from the clay minerals (Fig. 6). We suggest that these data would also apply to other shales with comparable contents of swelling clay minerals and thus comparable specific surface areas.

Specimen preparation and experimental configuration

Three different kinds of specimens of Opalinus shale were deformed: intact rock samples with layering parallel to σ_1, intact rock samples with layering normal to σ_1, and sintered specimens.

The cored rock samples showed a porosity of 10%. To prepare the sintered specimens, Opalinus shale was crushed and the sieved fraction (<125 μm) was mixed with 12 weight % water. Sintering under an isostatic pressure of 5 MPa at room temperature resulted in cohesive cylinders with 20% porosity. After drying at 105°C for 24 h, the water content is nearly zero (theoretical value). As hydrating started immediately after removal from the drying apparatus, standard sealing procedures resulted in samples with approximately 1.8% water content. A 0.4% water-content specimen was manufactured for one test series (Fig. 8). An approximate water content of 1.8% was also shown by cored rock samples that were dried and sealed the same way.

The experiments were performed in a triaxial deformation apparatus, described by Müller & Briegel (1977), at confining pressures (cp) ranging from 0.1 to 400 MPa, at temperatures from 20 to 350°C and at strain rates from 10^{-4} to $10^{-6}\ s^{-1}$. Most of the samples and specimens were strained in a coaxial configuration. Simple shear experiments were performed on shale gouges between limestone cylinders precut at an angle of 35° to the shortening direction using a configuration similar to that described by Friedman & Higgs (1981).

Mechanical observations

The strength of dry sintered specimens and rock samples (1.8 weight % water) was generally independent of strain rate but dependent on confining pressure. The sintered specimens compacted during the experiments resulting in a decrease of porosity from 20 to 10%. On the other hand, cored rock samples showed dilatation (e.g. 7% at 30% strain and 50 MPa cp). The intact rock samples deformed with σ_1 parallel to the layering showed higher cohesion (34.4 MPa) and internal friction ($\phi = 14.5°$) than those with σ_1 normal to layering ($c = 29.8$ MPa, $\phi = 13.6°$) corresponding to the results of Donath (1961). The cohesion of sintered samples is 16.3 MPa with internal friction $\phi = 27.4°$.

Up to 200°C, the strength of the sintered specimens (with 1.8% water) deformed at strain rates of $10^{-4}\ s^{-1}$ is independent of temperature (Fig. 7). Experiments at temperatures above 200°C indicate stick–slip, which we suggest is caused by increasing embrittlement as a result of dewatering (drained experiments). The corresponding maximum strength values show strong scattering,

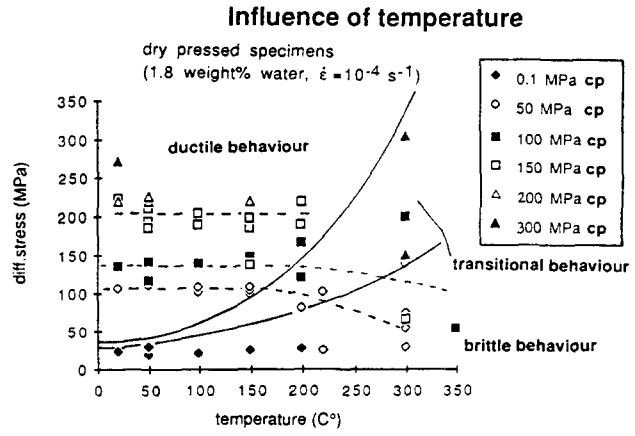

Fig. 7. Strength of sintered 'dry' (1.8% water) specimens at 10% strain vs temperature. Up to 200°C, strength is independent of temperature. Experiments above 200°C indicate stick–slip, dewatering and embrittlement.

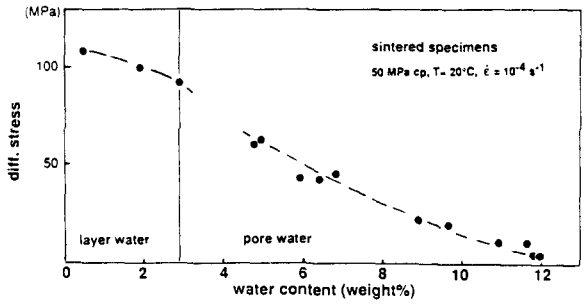

Fig. 8. Strength of sintered specimens at 10% strain vs water content.

probably caused by variations in the amount of dewatering from specimen to specimen. Generally, with increasing temperature the deformation regime changes from more or less cataclastic ('ductile') to transitional and brittle behavior (Fig. 7).

The influence of water was investigated in experiments on sintered samples with known water contents ranging from 0.4–12% (Fig. 8), with all other ambient conditions fixed. At 50 MPa cp, *ca* 2.8 weight % water is adsorbed (cf. Fig. 6), and excess water is denoted as pore water. It can be shown that variations in layer water (from undersaturated to saturated) have a distinct influence on bulk strength. A small increase in pore water content from 2.8 to 5% reduces the bulk strength by 30%. Although the specimens were drained, pore pressure built up within them (see below) that, depending on absolute water content, came close to the confining pressure.

Sintered specimens manufactured from different sieve fractions show the influence of variations in mineral composition to be moderate. Reduction of clay mineral content from 90 to 10% in favor of a polymineralic silt fraction (quartz, feldspar, micas, etc.) resulted in a strength increase of only 20%. Nevertheless, differences in strength of the differing mineralogies is significant in that strain is concentrated within the clay-rich part of those deformed rock samples with lithological anisotropies.

Microstructural observations

In the following we mainly concentrate on coaxially deformed rock samples (1.8 weight % water) with layering parallel to σ_1. At 0.1 MPa cp a combined pattern of extension fractures and shear fractures is formed. The crushed zone of about 1 mm width in the lower part of the specimen indicates particle size reduction (Fig. 9a). The corresponding stress–strain curve shows brittle failure. At 25 MPa cp and higher, all samples show propagating conjugate kink bands that are cut by subsequent sub-parallel (*R*-type) shear fractures. The kink bands become broader with increasing confining pressure. All deformation curves from 25 to 150 MPa show brittle failure (Fig. 9), followed by stick–slip at lower stress

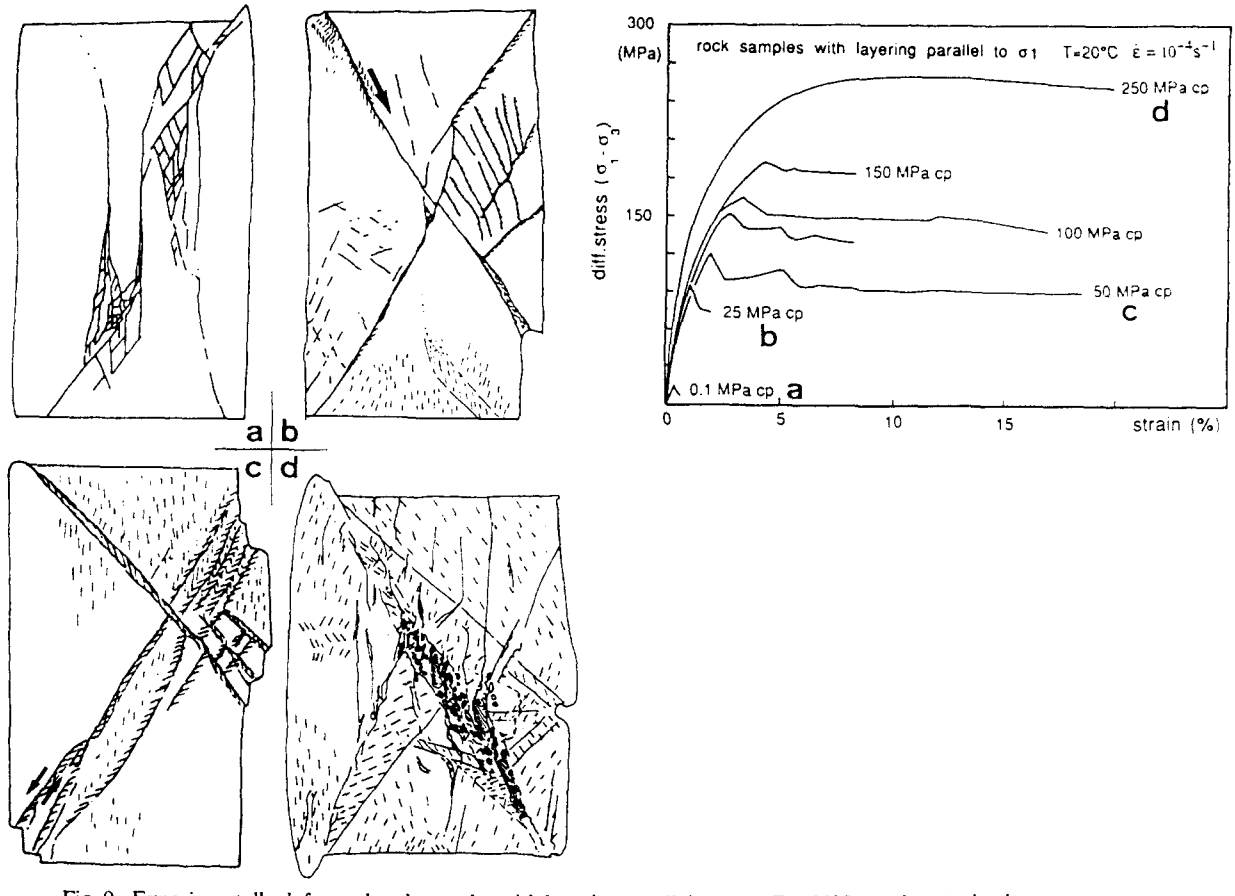

Fig. 9. Experimentally deformed rock samples with layering parallel to σ_1 at $T = 20°C$ and $\dot{\varepsilon} = 10^{-4}\,s^{-1}$; (a) 0.5% strain at 0.1 MPa cp; (b) 9% strain at 25 MPa cp; (c) 19% strain at 50 MPa cp; (d) 22% strain at 250 MPa cp and corresponding stress–strain curves.

levels. This coincides with the observations of Jackson & Dunn (1974).

At 25 MPa cp, two dominant shear fractures with a subordinate network of extension fractures developed and overprinted very small (0.1 mm) kink bands. At 50 MPa cp, a system of conjugate kink bands (1 mm wide) developed. With increasing strain, the kink system propagated in the form of alternating conjugate kink bands in the direction of the smallest quadrant of the sample (eastern quadrant in Fig. 9c). At 100 MPa cp (Figs. 4a–c), the kink zones were about 3 mm wide and were overprinted by *R*- and *P*-shears after a maximum kink angle was reached (Fig. 4c). Even the smallest part of the sample bordered by two shear factures showed a pervasive kinking (Fig. 4b).

At 250 MPa cp the kink band widened from the rim of the sample towards the core (Fig. 9d). This configuration depends upon the pressure shadow due to the experimental rig. The development of rounded clasts in kink bands is noteworthy. The corresponding stress–strain curve shows transitional behavior.

The coaxially deformed wet specimens (>1.8% water) differ in overall shape from 'dry' ones. Generally, deformation is 'ductile', i.e. pervasive cataclasis is favored by the presence of water. Sintered samples with adsorbed layer water are deformed ductilely throughout, resulting in a barrel-shaped form. All specimens with free pore water are 'vase'-shaped (i.e. they bulge at the undrained end) indicating that the pore pressure could not dissipate through the sample to the drained end during the experiment. Therefore, we suggest that crushed shale rock flours can reduce the permeability as has been suggested for clay gouges (Morrow *et al.* 1984). Figure 4(d) shows a sinistrally deformed clay gouge with 30% water. The clay minerals were originally subparallel to the border of the precut limestone. During deformation some clay minerals were kinked (K) and developed a foliation normal to bulk σ_1. This foliation was cut by *R*-shears (R), which are now subparallel to the shear zone. Sliding on bound water layers is suggested to be common on *R*-shear surfaces. Nevertheless, despite the high water content, deformation is also accommodated by kinking and shearing as in the 'dry' specimens. This is in accordance with observations in wet shale and clay by Riedel (1929), Maltman (1987) and others.

In summary, kinking and shearing on *R*- and *P*-surfaces, and sliding on water interlayers (*R*-surfaces) are the most important deformation mechanisms in shales. Under all experimental conditions utilized, shales do not leave the brittle field. Nevertheless, samples with high water content show low-strength pseudo-viscous pervasive cataclasis ('clay plasticity') at low temperatures and low confining pressures. At high temperatures and high confining pressures water is forced out, provided drainage is possible, and the samples behave like a 'dry' specimen. We propose this deformation mechanism to be responsible for shale deformation at near surface conditions (<150 m), e.g. within sliding horizons of large landslides. In contrast, deformation in low water ('dry') specimens is increasingly focused on discrete shear surfaces as strain increases. With increasing confining pressure, the initial (cataclastic) kink bands become broader and the number of slickensides increases. This results in a more ductile (cataclastic) behavior. Nevertheless, cataclasis never becomes really pervasive, because increasing confining pressure as well as increasing temperatures causes dewatering which results in embrittlement and so an increase of internal friction.

DISCUSSION

Field vs experimental evidence

Experimental results confirm the existence in the subsurface of a regime of low-strength pervasive cataclasite-type deformation in shales not known in other rock types. The existence of such a deformation regime can be explained by particularities of shales, mainly the ability of clay minerals to adsorb and to hold water. This layer water decreases the strength of clay and therefore of shales significantly even, as we suggest, when no excess pore pressure is built up. Furthermore, at higher strain rates, the ability of shales to reduce permeability may result in local excess pore pressures. At slow strain rates, we presume that drainage occurs even in shales, due to the presence of fractures and silty interlayers. Within evaporites, the cataclasitic-type deformation becomes ductile due to the precipitation of gypsum within the dilatation-induced pore space. Petrological, chemical and/or structural particularities depress the onset of deformation of this type to a greater depth than that at which it occurs in shale formations.

The experimental evidence is that in 'dry' specimens strain is focused on slickensides as strain increases, although deformation starts as kink bands (in agreement with field observations from deformation regimes of greater depth). Obviously, the onset of pervasive cataclasis is shifted to increasingly greater depths as water is successively forced out by ambient pressure and temperature, resulting in a progressive increase of cohesion and internal friction (ϕ), while the values for 'external friction' on slickensides stay more or less constant. This explains the absence of pervasive shale cataclasites within the Jura overthrust. Even at depths greater than 1.5 km, strain within shales is concentrated on discrete surfaces (Matter *et al.* 1988).

Inversion of relative competence in the light of experimental work

The inversion of relative competence of shales and anhydrite observed within the evaporite shear zones of the Jura can be explained by reference to a simple compilation of experimental data (Fig. 10). We used the experimental data on the mechanical behavior of shales (Nüesch 1989), anhydrite (Müller & Briegel 1978, Müller *et al.* 1981), and gypsum (Baumann 1984). The data are presented in a plot of depth vs strength. Tem-

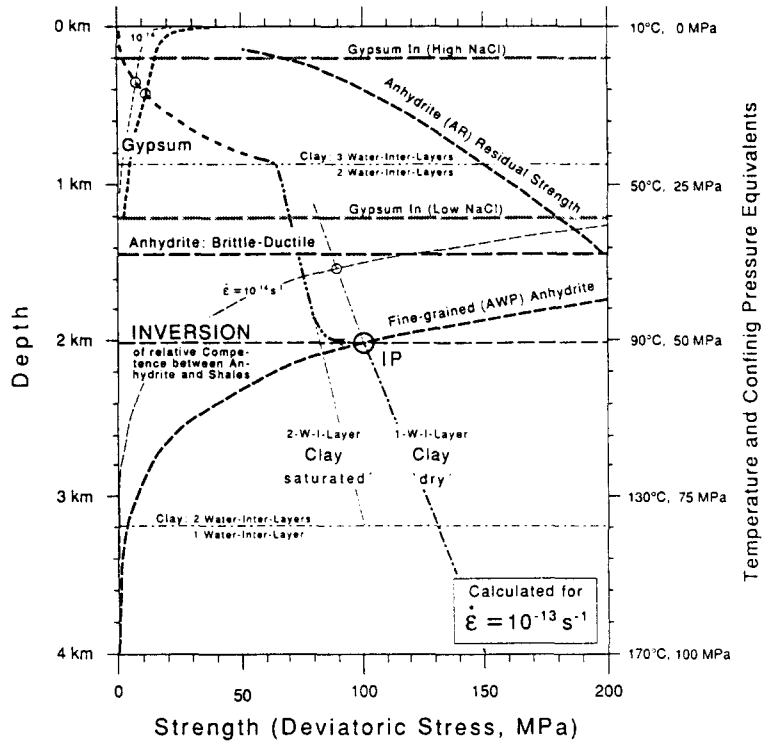

Fig. 10. Compilation of mechanical data of shales, anhydrite and gypsum calculated for the ambient conditions of Jura overthrusting. This compilation provides a qualitative explanation for inversion of relative competence of anhydrite and shales (IP = inversion point) and for the occurrence of three (or four) different deformation regimes and consequent patterns (see text).

perature and confining pressure are directly related to depth, assuming a surface temperature of 10°C, a geothermal gradient of 40°C km^{-1} (Diebold & Müller 1985), and a specific weight of the overburden of 2.5 g cm^{-3}. The plot is constructed for strain rates of $\dot{\varepsilon} = 10^{-13}$ s^{-1} (heavy lines) and $\dot{\varepsilon} = 10^{-14}$ s^{-1} (fine lines). Deformation rates are taken as pure shear instead of simple shear for an easier comparison with published rock mechanics data. Qualitatively, there is no significant difference between a pure and a simple shear compilation. Quantitatively a factor of 1.74 has to be introduced (Nye 1953, Jordan 1987, Schmid *et al.* 1987), causing a stretching along the horizontal axis of the plot. However, this factor is well below other uncertainties and so it is ignored here. We used a combination of two tested lithologies in order to get the lowest strength of anhydrite under all conditions, i.e. for the ductile domain and the brittle–ductile transition we used the AWP-data (fine-grained anhydrite of Wandflue type, deformed parallel to layering), and for the residual strength we used the AR-data (medium-grained anhydrite of Ryburg type, cf. Müller & Briegel 1978, Müller *et al.* 1981) (Table 1). The mechanical data for shales are from a combination of various clay deformation experiments. Primarily, we calculated a strength–depth curve for 'saturated' clay minerals, assuming no additional pore pressure. Additionally, within the stability field of 2-WIL (water-interlayer) clay, we also calculated the curve for 1-WIL clay, assuming that 1-WIL clay survives as a semi-stable configuration during syntectonic denudation, provided that the system is closed. These curves give maximum strength values only, since strength can be significantly reduced by the presence of pore pressure. For the gypsum–anhydrite equilibrium the data of Berner (1971) were used.

The compilation predicts an inversion of competence (i.e. of relative strength of shale (clay) and anhydrite) at the inversion point IP on Fig. 10, although all potential mutual chemical and mechanical effects of interaction of the several lithologies involved, such as anhydrite veins in shales, gypsification, etc., are excluded. Assuming that the shifting of the accommodation of bulk tectonic movements from anhydrite to shales causes a breaking up of an originally closed system, resulting in a sudden hydration of the undersaturated 1-WIL swelling clay-minerals (see above), a stress drop within shales has to be expected, which is indicated in the compilation.

The depth of *ca* 2 km (at $\dot{\varepsilon} = 10^{-13}$ s^{-1}) predicted for the inversion point, however, does not agree with field evidence that yields an inversion at *ca* 600 m. We suggest that there are various possibilities to explain this discrepancy. There are several uncertainties in extrapolation of field data toward low stresses. Furthermore, in compiling the plot, all interactions between the involved lithologies have been deliberately omitted. Now, adjusting for all factors that result in a correction of shale strength toward lower stresses, like excess pore water, strain dependency of pore water influence and sulfate lubrication, brings the inversion point toward even greater depths. On the other hand, all factors 'reducing' the anhydrite strength, like additional pressure solution (Laubscher 1984) and low-strength deformation mechanisms, not yet detected in laboratory experiments, would tend to reconcile the plot with field evidence.

Likewise correction of deformation rate estimates toward lower strain rates would shift the inversion point toward shallower depths. However, in the present plot, even when unrealistically slow strain rates of $\dot{\varepsilon} = 10^{-15}$ s^{-1} are assumed, competence inversion is predicted at depths of greater than 1 km. Finally, this model is based on a threefold system of shales, anhydrite and gypsum, which does not correspond fully with nature where, for example, the presence of dolomite has an obvious influence on the rheological behavior of shales as well as that of anhydrite. In both cases, an increase in dolomite content causes increasing strength. However, considering that dolomite is more abundant within the shales than within the sulfates, no significant modification of the compilation is to be expected.

In summary, the compilation of data in Fig. 10 gives a good qualitative overview of deformation regimes in evaporite shear zones. Nevertheless, for quantitative estimates, further experimental and field work has to be done, especially in the area of anhydrite deformation. The plot gives a good overview of the three deformation regimes. Regime 1 can be localized at depths below the inversion point. Regime 2 corresponds to the region between the inversion point and the point of dramatic drop in strength of shales, which is preceded by or, in naturally deformed evaporites may coincide with, the brittle–ductile transition of anhydrite and the onset of gypsification. Regime 3 is restricted to an even shallower domain. There is some evidence that under subsurface conditions, gypsum behaves brittlely, and is more competent than shales. This fourth deformation regime would correspond to the uppermost 400 m in Fig.10.

CONCLUSIONS

In the shale–evaporite multilayers of evaporite shear zones in the Jura, three deformation patterns can be recognized. They result from variations in relative competence, deformation mechanisms and water access. Qualitatively, the three deformation regimes that produced these patterns can be simulated by a simple compilation of experimental data.

In a strict sense, shales behave brittlely under all ambient conditions encountered in nature and experiment. One can distinguish between a domain in which strain is focused within narrow shear zones aligned in a well-defined geometry (*"Y"–"R"*, etc.) and a domain with cataclasite-type deformation. Contrary to classical rock behavior, the latter pervasive deformation regime is found at shallow depth, while the former is restricted to deeper domains. The 'true' cataclastic zone of shale deformation (connected to high ambient pressures) is only found in room temperature experiments. In the first domain, slickensides develop from kink- or drag-like shear zones. This development coincides with a size reduction and a progressive alignment of clay aggregates parallel to the shear zone. Within the shale interlayers of the evaporites, the slickensides may be coated by secondary sulfate that acts as a lubricant. The onset of pervasive deformation in the second domain is strongly related to the penetration of water and decreasing ambient pressure. The resulting very low-strength 'shale–gypsum-tectonites' are the lubricants of the shallow part of Jura overthrust. In sulfate-free Opalinus shales, however, pervasive deformation is restricted to even shallower depths ('shale-plasticity').

In summary, the three questions outlined at the beginning of the paper can be answered in the following way: (1) the decisive peculiarity of shale deformation in evaporites is sulfate lubrication, which not only reduces the strength but also influences the deformational behavior of shales, e.g. depresses the onset of the subsurface type of pervasive cataclasis ('shale–gypsum-tectonites'); (2) shale deformation outside evaporites is generally friction-controlled, within evaporites, sulfate lubrication reduces the amount of friction; (3) within the shallow domain, shales have a lasting influence on bulk deformational behavior of evaporite detachments and décollements (taking over of bulk shear movements by shales and 'shale–gypsum-tectonites' when anhydrite becomes brittle).

Acknowledgements—We wish to thank H. Laubscher, W. H. Müller, W. Baumann and S. Schmid for stimulating discussions on evaporite detachment. Comments by Dave Olgaard and reviews by P. F. Williams, J. G. Spray and an anonymous reviewer greatly improved the paper. Research was partly supported by Swiss National Foundation, grant 3387 and 2.324-0.86. Experimental work was performed in K. J. Hsü Laboratory of Experimental Geology at ETH. Sandra Eugster and Dave Olgaard are acknowledged for improving our English.

REFERENCES

Baumann, W. 1984. Rheologische Untersuchungen an Gips. *Eclog. geol. Helv.* **77**, 301–325.

Becker, A., Blümling, P. & Müller, W. H. 1987. Recent stress field and neotectonics in the eastern Jura Mountains, Switzerland. *Tectonophysics* **135**, 277–288.

Berner, R. A. 1971. *Principles of Chemical Sedimentology*. McGraw-Hill, New York.

Buxtorf, A. 1907. Zur Tektonik des Kettenjura. *Ber. Versamml. oberrh. geol. Ver.*, **30/40**, 29–38.

Byerlee, J. D. 1978. Friction of rocks. *Pure & Appl. Geophys.* **116**, 615–633.

Carter, N. L. & Hansen, F. D. 1983. Creep of rocksalt. *Tectonophysics* **92**, 275–333.

Chappell, B. A. 1974. Deformational response of differently shaped and sized test pieces of shale rock. *Int. J. Rock Mech. Min. Sci. & Geomech. Abs.* **11**, 21–25.

Cooper, B. N. 1970. The Max meadow breccias: a reply. In: *Studies of Appalachian geology: Central and Southern* (edited by Fisher, G. W., Pettijohn, F. J., Reed, J. C. & Weaver, K.N.). Wiley, New York, 179–191.

Davies, M. D. & Engelder, J. T. 1985. The role of salt in fold-and-thrust belts. *Tectonophysics* **119**, 67–88.

Diebold, P. & Müller, W. H. 1985. Szenarien geologischer Langzeitsicherheit: Risikoanalyse für ein Endlager für hochradioaktive Abfälle in der Nordschweiz. *NTB* **84-26**, NAGRA, Baden.

Donath, F. A. 1961. Experimental study of shear failure in anisotropic rocks. *Bull. geol. Soc. Am.* **72**, 985–990.

Friedman, M. & Higgs, N. G. 1981. Calcite fabrics in experimental shear zones. *Am. Geophys. Un. Geophys. Monogr.* **24**, 11–27.

Handin, J., Hager, R. V., Jr., Friedman, M. & Feather, J. N. 1963. Experimental deformation of sedimentary rocks under confining pressure: pore pressure tests. *Bull. Am. Ass. Petrol. Geol.* **47**, 717–748.

Harland, W. B., Mann, A. & Townsend, C. 1988. Deformation of anhydrite–gypsum rocks in central Spitsbergen. *Geol. Mag.* **125**, 103–116.

Harris, L. D. & Milici, R. C. 1977. Characteristics of thin-skinned style of deformation in the Southern Appalachians, and potential hydrocarbon traps. *Prof. Pap. U.S. geol. Surv.* **1018**.

Heard, H. C. 1972. Steady-state flow in polycrystalline halite at pressure of 2 kilobars. *Am. Geophys. Un. Geophys. Monogr.* **16**, 191–209.

Helman, M. R. & Schreiber, B. C. 1983. Permian evaporite deposits of the Italian Alps (Dolomites): the development of unusual and significant fabrics. *Sixth Int. Symp. on Salt* **1**, 57–66.

Hsü, K. J. 1979. Thin-skinned plate tectonics during neo-Alpine orogenesis. *Am. J. Sci.* **279**, 353–366.

Jackson, R. E. & Dunn, D. E. 1974. Experimental sliding friction and cataclasis of foliated rocks. *Int. J. Rock Mech. Min. Sci. & Geomech. Abs.* **11**, 235–249.

Jordan, P. 1987. Eine Methode zur Abschätzung tektonischer Scherraten aufgrund mikrostruktureller Beobachtungen. *Eclog. geol. Helv.* **80**, 491–508.

Jordan, P. 1988. Deformationsverhalten der Keuper Evaporite des Belchen-Tunnels (Faltenjura, Schweiz). *Erlanger geol. Abh.* **116**, 53–66.

Jordan, P. & Nüesch, R. 1989. Deformation structures in the Muschelkalk Anhydrites of the Schafisheim Well (Jura Overthrust, Northern Switzerland). *Eclog. geol. Helv.* **82**, 429–454.

Laubscher, H. P. 1961. Die Fernschubhypothese der Jurafaltung. *Eclog. geol. Helv.* **54**, 221–282.

Laubscher, H. P. 1973. Jura Mountains. In: *Gravity and Tectonics* (edited by De Jong, K. A. & Scholten, R.). Wiley, London, 217–227.

Laubscher, H. P. 1976. Viscous components in Jura folding. *Tectonophysics* **27**, 239–254.

Laubscher, H. P. 1977. Fold development in the Jura. *Tectonophysics* **37**, 337–362.

Laubscher, H. P. 1978. Foreland folding. *Tectonophysics* **47**, 325–337.

Laubscher, H. P. 1984. Sulfate deformation in the upper Triassic of the Belchen tunnel (Jura Mountains, Switzerland). *Eclog. geol. Helv.* **77**, 249–259.

Laubscher, H. P. 1986. The eastern Jura: relations between thin skinned and basement tectonics, local and regional. *Geol. Rdsch.* **75**, 535–553.

Logan, J. M., Higgs, N. G. & Friedman, M. 1981. Laboratory studies on natural gouge from the U.S. Geological Survey Dry Lake Valley No. 1 Well, San Andreas Fault zone. *Am. Geophys. Un. Geophys. Monogr.* **24**, 121–134.

MacDonnald, R. 1953. Anhydrite–gypsum equilibrium relations. *Am. J. Sci.* **251**, 884–898.

Madsen, F. T. & Müller-Vonmoos, M. 1985. Swelling pressure calculated from mineralogical properties of a Jurassic opalinum shale, Switzerland. *Clays Clay Minerals* **33**, 501–509.

Maltman, A. 1984. On the term 'soft-sediment deformation'. *J. Struct. Geol.* **6**, 589–592.

Maltman, A. 1987. Shear zones in argillaceous sediments—an experimental study. *Spec. Publs geol. Soc. Lond.* **29**, 77–87.

Marcoux, J., Brun, J. P., Burg, J.-P. & Ricou, L. E. 1987. Shear structures in anhydrite at the base of thrust sheets (Antalya, Southern Turkey). *J. Struct. Geol.* **9**, 555–561.

Matter, A., Peters, Tj., Bläsi, H-R., Schenker, F. & Weiss, H.-P. 1988. Sondierbohrung Schafisheim: Geologie. *NTB* **86-03**, NAGRA, Baden.

Morrow, C. A., Shi, L. Q. & Byerlee, J. D. 1984. Permeability of fault gouge under confining pressure and shear stress. *J. geophys. Res.* **89**, 3193–3200.

Müller, W. H. & Briegel, U. 1977. Experimentelle Untersuchungen an Anhydrit aus der Schweiz. *Eclog. geol. Helv.* **70**, 397–407.

Müller, W. H. & Briegel, U. 1978. The rheological behaviour of polycrystalline anhydrite. *Eclog. geol. Helv.* **71**, 397–407.

Müller, W. H., Huber, M., Isler, A. & Kleboth, P. 1984. Erläuterungen zur "Geologischen Karte der zentralen Nordschweiz 1 : 100 00". *NTB* **84-25**, NAGRA, Baden.

Müller, W. H. & Hsü, K. J. 1980. Stress distribution in overthrusting slabs and mechanics of Jura deformation. *Rock Mech., Suppl.* **9**, 219–232.

Müller, W. H., Schmid, S. M. & Briegel, U. 1981. Deformation experiments on anhydrite rocks of different grain sizes: rheology and microfabric. *Tectonophysics* **78**, 527–543.

Mullis, J. 1987. Fluideinschluss-Untersuchungen in den Nagra-Bohrungen der Nordschweiz. *Eclog. geol Helv.* **80**, 553–568.

Mullis, J. & Stalder, H. A. 1987. Salt-poor and salt-rich fluid inclusions from two boreholes in northern Switzerland. *Chem. Geol.* **61**, 263–272.

Nüesch, R. 1989. Felsmechanische Resultate aus Untersuchungen an Opalinuston. Unpublished Ph.D. thesis, ETH Zürich, Switzerland.

Nüesch, R. & Baumann, W. 1989. Ton- und Sulfatgesteine in Wechselwirkung bei Deformation. *Geol. Rdsch.* **78**, 443–457.

Nye, J. F. 1953. The flow-law of ice from measurements in glacier tunnels, laboratory experiments and the Jungfrau borehole experiment. *Proc. R. Soc. Lond.* **219**, 477–489.

Peters, Tj., Matter, A., Bläsi, H-R. & Gautschi, A. 1986. Sondierbohrung Böttstein: Geologie *NTB* **85-02**, NAGRA, Baden.

Prasad, N. 1970. Sedimentology of Keuper from the Belchentunnel – Eastern Swiss Jura. Unpublished Ph.D. thesis, University of Basel, Switzerland (short version published 1974).

Ramsay, J. G. 1981. Tectonics of the Helvetic nappes. In: *Thrust and Nappe Tectonics* (edited by McClay, K. R. & Price, N. J.). *Spec. Publs geol. Soc. Lond.* **9**, 293–309.

Riedel, W. 1929. Zur Mechanik geologischer Brucherscheinungen. *Zentbl. Miner. Geol. Paläont.* **1929b**, 354–368.

Rutter, E. H., Maddock, R. H., Hall, S. J. & White, S. H. 1986. Comparative microstructures of natural and experimentally produced clay bearing fault gouges. *Pure & Appl. Geophys.* **124**, 3–30.

Rutter, E. H. & White, S. H. 1979. The microstructures and rheology of fault gouges produced experimentally under wet and dry conditions at temperatures up to 400°C. *Bull. Mineral.* **102**, 101–109.

Schmid, S. M., Panozzo, R. & Bauer, S. 1987. Simple shear experiments on calcite rocks: rheology and microfabrics. *J. Struct. Geol.* **9**, 747–778.

Summers, R. & Byerlee, J. 1977. A note on the effect of fault gouge composition on the stability of frictional sliding. *Int. J. Rock Mech. Min. Sci. & Geomech. Abs.* **14**, 155–160.

Urai, J. 1985. Water enhanced dynamic recrystallization and solution transfer in experimentally deformed carnallite. *Tectonophysics* **120**, 285–317.

van Berkel, J. T., Torrance, J. G. & Schwerdtner, W. M. 1986. Deformed anhydrite nodules: a new type of finite strain gauge in sedimentary rocks. *Tectonophysics* **124**, 309–323.

Wang, C., Mao, N. & Wu, F. T. 1980. Mechanical properties of clays at high pressure. *J. geophys. Res.* **85**, 1462–1468.

Wohnlich, H. M. 1967. Kleintektonische Bruch- und Fliessdeformation im Faltenjura. Unpublished Ph.D. thesis, University of Basel, Switzerland.